Torque Improvement of Spoke-type Permanent Magnet Motor with Auxiliary Stator Using Harmonic Current Control Strategy

Hao Wu, Wenliang Zhao, *Member, IEEE,* Zheng Li, and Xiuhe Wang

***Abstract*—The spoke-type permanent magnet motor with auxiliary stator exhibits high torque performance owing to the flux focus effects. To further improve its torque density, this paper proposes a control method by using harmonic current strategy. Based on the theoretical analysis, a 3-D torque look-up table by *dq*-axis current and electrical angle is established with the aid of the finite element method (FEM). The maximum torque per ampere curve at each rotor position is identified and summarized to adequately indicate the relationship between torque and current amplitude of the motor. Through theoretical derivation, it is concluded that the minimum torque cost curve is the contour line of $\partial T_e/\partial i^2$, which can be employed to identify the harmonic current for torque density improvement. Compared to traditional strategies, the proposed control strategy can increase torque density of forward and reverse torque by 1.22% and 1.40%, respectively. The experimental results verify the analysis and simulation results, as well as prove the effectiveness of the proposed strategy.**

***Index Terms*—Spoke-type permanent magnet motor, Harmonic current, Finite element method, Torque density, Torque cost.**

I. Introduction

In recent years, the permanent magnet synchronous motor has been widely used in new energy vehicles, industrial production and many other fields due to its advantages such as simple structure, flexible control, and high reliability [1]-[5]. Among them, the spoke-type permanent magnet (PM) motor has high efficiency and torque density benefiting from the concentrated flux from rotor magnets [6]-[8], which is regarded as a good candidate for distributed drive systems, particularly in the development direction of in-wheel motor drive for electric vehicles [9]-[11].

In general, the distributed drive systems require the highest possible torque density. To improve the torque density of the spoke-type PM motor, the design-based or control-based strategies can be used. At the control level, for higher torque densities, the rated current is usually set to the current value at the maximum current density, and higher current will burn out the motor windings [12]-[13]. Therefore, the improvement of torque density is equivalent to seeking a higher torque per ampere (TPA). Conventionally, the maximum torque per ampere (MTPA) operating point is identified by constant motor parameters, but no variation in motor parameters is considered [14]-[15]. Some predefined equations with current as a variable are used to calculate the MTPA operating point, but the effect of the rotor position angle and the derivative term of the motor parameters is not considered [16]-[18]. Simplifying functions are used to approximate the MTPA curve, but the full potential of motor is not used [19]-[21]. The harmonic current injection is considered as an effective solution to enhance performance of the system [12], [22]-[25]. Based on multi-objective optimization algorithm, a strategy is proposed to identify the amplitude of the injected harmonics to improve the torque density, but only the 3rd, 5th, 7th and 9th harmonics were considered [12]. In [12], a spoke-type PM motor with the auxiliary stator is presented to improve torque density and suppress torque pulsations, but only limited to the topology design level.

In this paper, to further improve the torque performance of the spoke-type PM motor with auxiliary stator, the control strategy by using the harmonic current is proposed. Taking into account the cross-coupling, magnetic saturation, and magnetic field harmonics, the theoretical derivations are implemented to summarize the torque response law. A mathematical model isestablished to represent the torque response. Then the maximum value of the average torque output is found, while the conditions for this value to be satisfied are given, and the harmonic currents are thereby identified. The finite element method (FEM) is first utilized to validate the proposed harmonic current injection strategy. Finally, the experiments are carried out to verify the analysis and simulation results.

II. Mathematical Modeling of the Spoke-Type PM Motor

Fig. 1 shows the topology structure of the spoke-type PM motor, which is composed of an outer stator, an auxiliary inner stator, windings, rotor cores and permanent magnets. The parameters of the spoke-type PM motor are shown in Table I.

TABLE I
PARAMETERS OF SPOKE-TYPE PM MOTOR

Symbol	Item	Unit	Value
p	Number of pole pairs	-	13
R	Phase resistance	Ω	0.17
I_N	Rated current	A	26.72
L^c_d	Direct axis inductance of conventional model	mH	1.8

Manuscript received August 03, 2022; revised October 02, 2022; accepted October 21, 2022. Date of publication June 25, 2023; Date of current version January 17, 2023.

This work was supported in part by the National Natural Science Foundation of China under Grant 52077123 and 51737008, and in part by the Natural Science Foundation of Shandong Province of China for Outstanding Young Scholars, under Grant ZR2021YQ35. (*Corresponding author: Wenliang Zhao.*)

H. Wu, W. Zhao and X. Wang are with the School of Electrical Engineering, Shandong University, Jinan, 250061, China(e-mail: haowu20211998@163.com; wlzhao@sdu.edu.cn; wangxh@ sdu.edu.cn).

Z. Li is with the Jinan Heating Group CO. LTD, Jinan, 250011, China(e-mail: zhengli20231987@163.com).

Digital Object Identifier 10.30941/CESTEMS.2023.00022

L^c_q	Quadrature axis inductance of conventional model	mH	1.7
ψ_f	Permanent magnet flux linkage	Wb	0.0374

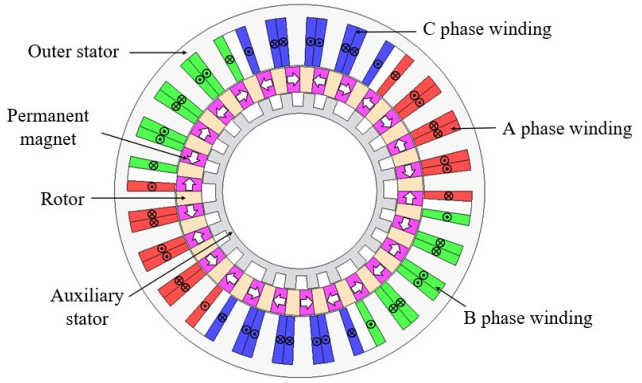

Fig. 1. Motor topology of the spoke-type PM motor.

A. Voltage Equations

In the rotor synchronous rotating coordinate system, the voltage equation can be expressed as

$$\boldsymbol{u} = R\boldsymbol{i} + \frac{\mathrm{d}}{\mathrm{d}t}\boldsymbol{\psi} + \omega_e \boldsymbol{T}\boldsymbol{\psi} \tag{1}$$

where

$$\boldsymbol{u} = \begin{bmatrix} u_d \\ u_q \end{bmatrix}, \boldsymbol{i} = \begin{bmatrix} i_d \\ i_q \end{bmatrix}, \boldsymbol{\psi} = \begin{bmatrix} \psi_d \\ \psi_q \end{bmatrix}, \boldsymbol{T} = \begin{bmatrix} 0 & -1 \\ 1 & 0 \end{bmatrix}$$

and u_d, u_q, i_d, i_q, ψ_d, ψ_q are the voltage, current, flux linkage of the motor at dq-axis, respectively; ω_e is the electrical angular velocity.

Assuming that it is an ideal situation condition, that is, there is no magnetic saturation, space harmonics and cross saturation effects. And there is $\psi_q \propto i_q$ and $(\psi_d - \psi_f) \propto i_d$, then

$$\begin{cases} u_d = Ri_d + L^c_d \dfrac{\mathrm{d}}{\mathrm{d}t} i_d - \omega_e L^c_q i_q \\ u_q = Ri_q + L^c_q \dfrac{\mathrm{d}}{\mathrm{d}t} i_q + \omega_e (L^c_d i_d + \psi_f) \\ T^c_e = \dfrac{3}{2} p i_q [i_d (L^c_d - L^c_q) + \psi_f] \end{cases} \tag{2}$$

Among them, T_e^c is the electromagnetic torque, and the superscript 'c' represents the conventional model. However, the actual situation is different from (2). Firstly, due to the existence of magnetic saturation, the change of flux linkage is not strictly proportional to the current. Secondly, due to the existence of cross-saturation effect, the change of i_q will change ψ_d, and the change of i_d will change ψ_q. Thirdly, due to the existence of harmonic magnetic fields generated by teeth and slots, $\boldsymbol{\psi}$ will vary with electrical angle of rotor position θ_e [26]. In short, the $\boldsymbol{\psi}$ is a function of the i_d, i_q and the rotor position, namely ψ_d (i_d, i_q, θ_e), ψ_q (i_d, i_q, θ_e). So, (1) is rewritten as

$$\begin{aligned} \boldsymbol{u} &= R\boldsymbol{i} + \frac{\partial \boldsymbol{\psi}}{\partial \boldsymbol{i}} \frac{\mathrm{d}}{\mathrm{d}t} \boldsymbol{i} + \omega_e \left(\frac{\partial \boldsymbol{\psi}}{\partial \theta_e} + \boldsymbol{T}\boldsymbol{\psi} \right) \\ &= R\boldsymbol{i} + \boldsymbol{L} \frac{\mathrm{d}}{\mathrm{d}t} \boldsymbol{i} + \omega_e (\boldsymbol{G} + \boldsymbol{T}\boldsymbol{\psi}) \end{aligned} \tag{3}$$

where

$$\boldsymbol{L} = \begin{bmatrix} L_d & L_{dq} \\ L_{qd} & L_q \end{bmatrix}, \boldsymbol{G} = \begin{bmatrix} \partial \psi_d / \partial \theta_e \\ \partial \psi_q / \partial \theta_e \end{bmatrix}$$

L_d, L_q are the self-inductance of the d-axis, q-axis; L_{dq}, L_{qd} are the mutual-inductance of the dq-axis.

B. Torque Equations

In the motor, the power P_{in} that inputs from the motor winding can be expressed as

$$\begin{aligned} P_{in} &= e_A i_A + e_B i_B + e_C i_C = \begin{bmatrix} i_A & i_B & i_C \end{bmatrix} \begin{bmatrix} e_A \\ e_B \\ e_C \end{bmatrix} \\ &= \begin{bmatrix} i_d & i_q \end{bmatrix} \boldsymbol{P}\boldsymbol{P}^T \begin{bmatrix} e_d \\ e_q \end{bmatrix} = \frac{3}{2} \begin{bmatrix} i_d & i_q \end{bmatrix} \begin{bmatrix} e_d \\ e_q \end{bmatrix} \\ &= \frac{3}{2} \begin{bmatrix} i_d & i_q \end{bmatrix} \boldsymbol{D}^{-1} \boldsymbol{D} \begin{bmatrix} e_d \\ e_q \end{bmatrix} = \frac{3}{2} (\boldsymbol{D}\boldsymbol{i})^T (\boldsymbol{D}\boldsymbol{e}) = \frac{3}{2} (\boldsymbol{D}\boldsymbol{i})^T \mathrm{d}(\boldsymbol{D}\boldsymbol{\psi}) \end{aligned} \tag{4}$$

where

$$P = \begin{bmatrix} \cos\theta_e & \cos(\theta_e - 2\pi/3) & \cos(\theta_e + 2\pi/3) \\ -\sin\theta_e & -\sin(\theta_e - 2\pi/3) & -\sin(\theta_e + 2\pi/3) \end{bmatrix}$$

$$\boldsymbol{D} = \begin{bmatrix} \cos\theta_e & -\sin\theta_e \\ \sin\theta_e & \cos\theta_e \end{bmatrix}, \boldsymbol{e} = \begin{bmatrix} e_d \\ e_q \end{bmatrix}$$

and i_A, i_B, i_C are the current of the three phase ABC; e_A, e_B, e_C are the electromotive force of the three phase ABC; e_d, e_q, are the electromotive force of the dq-axis.

According to the law of conservation of energy, the energy conversion in the spoke-type PM motor by ignoring the iron loss can be expressed as

$$\frac{3}{2} (\boldsymbol{D}\boldsymbol{i})^T \mathrm{d}(\boldsymbol{D}\boldsymbol{\psi}) = \frac{1}{p} T_e \mathrm{d}\theta_e + \mathrm{d}W \tag{5}$$

where

$$W = W_s + W_{iron}$$

W is the sum of magnetic field energy storage W_s and iron loss energy W_{iron}. The left-hand side of (5) is the input power of spoke-type PM motor, and the right-hand side of (5) is the output mechanical power and the variation of magnetic field energy, respectively. W_s can be expressed as

$$W_s = \int_V \left(\int \boldsymbol{H} \cdot \mathrm{d}\boldsymbol{B} \right) \mathrm{d}v \tag{6}$$

where $\boldsymbol{H}$ and $\boldsymbol{B}$ are magnetic field strength vector and magnetic field induction strength vector, respectively.

It can be obtained from (5) that

$$\mathrm{d}W = \frac{3}{2} \boldsymbol{i}^T \boldsymbol{L} \mathrm{d}\boldsymbol{i} + \left(\frac{3}{2} \boldsymbol{i}^T \boldsymbol{G} + \frac{3}{2} \boldsymbol{i}^T \boldsymbol{D}\boldsymbol{\psi} - \frac{1}{p} T_e \right) \mathrm{d}\theta_e \tag{7}$$

Therefore

$$\frac{\partial W}{\partial \theta_e} = \frac{3}{2} \boldsymbol{i}^T \boldsymbol{G} + \frac{3}{2} \boldsymbol{i}^T \boldsymbol{D}\boldsymbol{\psi} - \frac{1}{p} T_e \tag{8}$$

Hence

$$T_e = \frac{3}{2} p \boldsymbol{i}^T \boldsymbol{D}\boldsymbol{\psi} + \frac{3}{2} p \boldsymbol{i}^T \boldsymbol{G} - p \frac{\partial W}{\partial \theta_e} = T_{e1} + T_{e2} + T_{e3} \tag{9}$$

where

$$T_{e1} = \frac{3}{2} p \boldsymbol{i}^T \boldsymbol{D}\boldsymbol{\psi}, \quad T_{e2} = \frac{3}{2} p \boldsymbol{i}^T \boldsymbol{G}, \quad T_{e3} = -p \frac{\partial W}{\partial \theta_e}$$

Fig. 2 is the torque waveforms of T_{e1}, T_{e2}, T_{e3} and T_e under the condition that i_d=0 and i_q=$\sqrt{2}\, I_N$, where the d-axis is located at the centerline of the rotor core. It can be seen that T_{e1}, T_{e2}, T_{e3}

and T_e all contain components of torque pulsation, which are not accounted for in the conventional mathematical model.

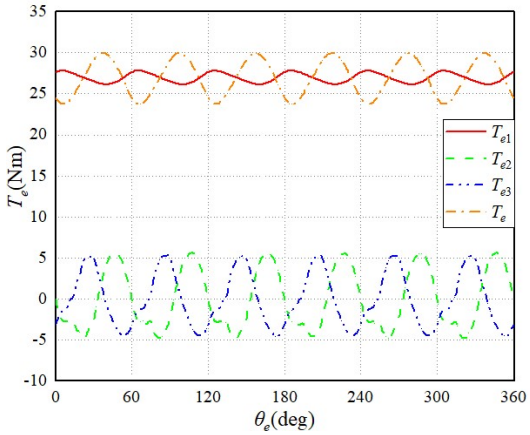

Fig. 2. Torque waveforms of each torque component.

C. Torque Cost

In the spoke-type PM motor, when constant $\boldsymbol{i}$ is employed to excitation, the copper losses P_{cu} can be expressed as

$$\begin{aligned} P_{cu} &= i_A^2 R + i_B^2 R + i_C^2 R \\ &= R\begin{bmatrix} \left(I\cos\theta_e\right)^2 + \left(I\cos(\theta_e - 2\pi/3)\right)^2 \\ + \left(I\cos(\theta_e + 2\pi/3)\right)^2 \end{bmatrix} \\ &= \frac{3}{2} I^2 R = \frac{3}{2}\left(i_d^2 + i_q^2\right) R \end{aligned} \tag{10}$$

where I is the amplitude of the $\boldsymbol{i}$. It can be seen from (10) that the heat dissipation of copper loss is proportional to the $\boldsymbol{i}^2$.

In the spoke-type PM motor, the torque density is limited by the heat generation of windings, that is, the magnitude of the $\boldsymbol{i}^2$. Therefore, the torque cost in this paper is defined as

$$\text{Torque cost} = \frac{\text{average}(\boldsymbol{i}^2)}{\text{average}(T_e)} \tag{11}$$

And it can be seen from (10) and (11) that when the $\boldsymbol{i}$ is constant, the torque fluctuates with the change of the θ_e, so the torque cost is variable. Therefore, it can be employed that variable $\boldsymbol{i}$ is injected at different θ_e to achieve the purpose of the torque density improvement.

III. Maximum Torque Density Model of the Spoke-type PM Motor

A. Torque Response Model

In the conventional strategy, increasing the torque density is achieved by making the motor work on the maximum torque per ampere (MTPA) curve. The curve satisfies the following conditions

$$\max\left(T_e / \sqrt{i_d^2 + i_q^2}\right) \tag{12}$$

The curve can be derived by equation (3), which is

$$\begin{cases} i_d = \dfrac{\psi_f}{2(L_d^c - L_q^c)} - \sqrt{\dfrac{\psi_f^2}{4(L_q^c - L_d^c)^2} + i_q^2} \\ i_q = \dfrac{\left(\dfrac{8T_e^c\psi_f}{3p}\right) + \sqrt{\left(\dfrac{8T_e^c\psi_f}{3p}\right)^2 - 4\left[\psi_f^2 - 4\left(L_d^c - L_q^c\right)^2\right]\left[\left(\dfrac{4T_e^c}{3p}\right)^2 - \psi_f^2\right]}}{2\left[\psi_f^2 - 4\left(L_d^c - L_q^c\right)^2\right]} \end{cases} \tag{13}$$

However, according to (3)-(9), the electromagnetic torque equation is a variable-parameter, multi-variable, high-order equation, which is more complex than conventional strategy and needs to be simplified. From (3)-(9), it can be seen that the motor torque T_e is a function of the variables ω_e, θ_e, and $\boldsymbol{i}$. However, since the effect of ω_e on T_e is negligible [16], [27-29], only the mapping of θ_e and $\boldsymbol{i}$ to T_e is considered. The 2-D

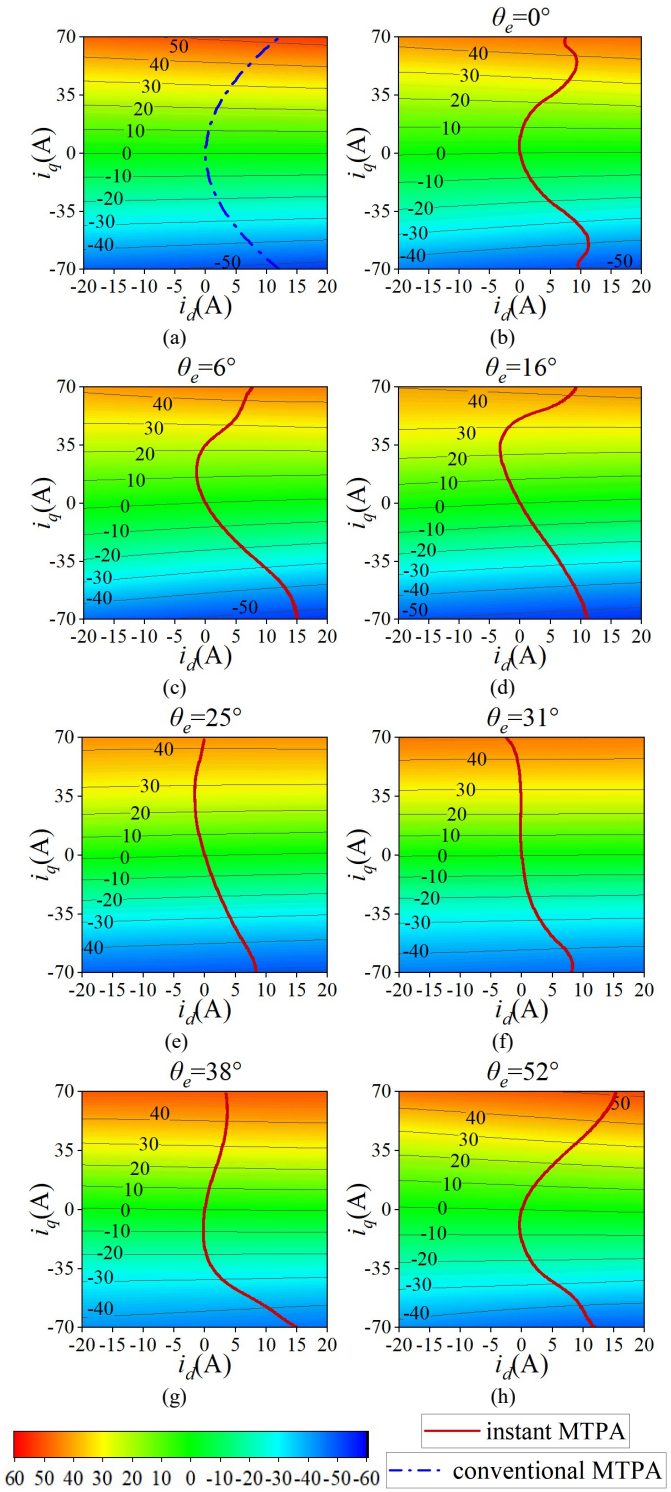

Fig. 3. Torque look-up table and MTPA curve.(a)conventional strategy (b) θ_e=0° (c) θ_e=6° (d) θ_e=16° (e) θ_e=25° (f) θ_e=31° (g) θ_e=38° (h) θ_e=52° (i) Color scale of torque value (j) Curve corresponding to the line type.

look-up tables identified by FEM can be employed to represent torque response as shown in Fig. 3 (b)-(h), which can form a 3-D look-up table. For comparison, the curve of the conventional strategy is plotted in Fig. 3(a).

In Fig. 3 (b)-(h), the seven sampling points (0°, 6°, 16°, 25°, 31°, 38°, 52°) are selected in an electrical angle cycle ($\theta_e \in [0°, 60°]$). The four points (6°, 25°, 38°, 52°) are selected near the extreme value points of rated torque and cogging torque, which makes the look-up table more accurate according to the interpolation principle, and the other three points are selected in the gap of the above four points. And the model can represent the motor torque effectively [28]. In order to reduce the heat generation of the motor, the MTPA curve at each sampling point is identified as the operating point according to the principle shown in Fig. 3 (b)-(h), which is named as instant MTPA curve. It can be found that the instant MTPA curves at different sampling points are significantly different, which can better consider the special conditions at each rotor position than the MTPA curves in Fig.3 (a). Because the current operating point that satisfies the minimum torque cost must be located on each instant MTPA curve, the minimum torque cost current must not operate at the constant (i_d, i_q) as the sine current in the ABC coordinate system, but the harmonic current.

B. The Principle of Minimum Torque Cost

Fig. 4 is a look-up table of forward T_e ($T_e \geq 0$), where the points satisfy

$$T_e(\theta_e, \boldsymbol{i}^2)\big|_{\text{minmum torque cost}} \tag{14}$$

where the MTPA curves at the seven θ_e sampling points are used to generate this table, and the values at non-sampling points are obtained using the interpolation method.

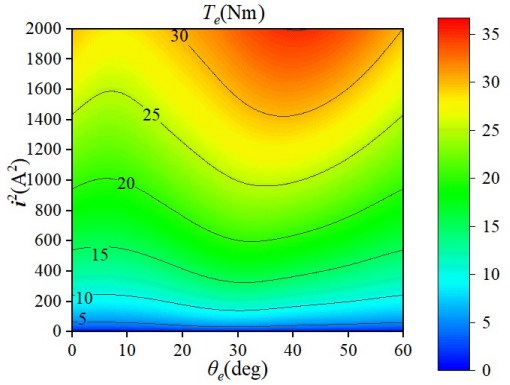

Fig. 4 Forward torque look-up table by θ_e and $\boldsymbol{i}^2$ lookup.

Fig. 5 is the lookup table of $\partial T_e / \partial \boldsymbol{i}^2$ calculated by Fig.4. It can be proved that the minimum torque cost curve is the contour line in Fig. 5. The proof process is as follows.

The contour line $f_1(\theta_e)$ and the non-contour line $f_2(\theta_e)$ are taken in a torque period, which satisfy

$$\int_0^{60} f_1(\theta_e)\mathrm{d}\theta_e / 60 = \int_0^{60} f_2(\theta_e)\mathrm{d}\theta_e / 60 \tag{15}$$

which means the average $\boldsymbol{i}^2$ is equal.

The difference F_1 of the T_e between the two curves can be expressed as

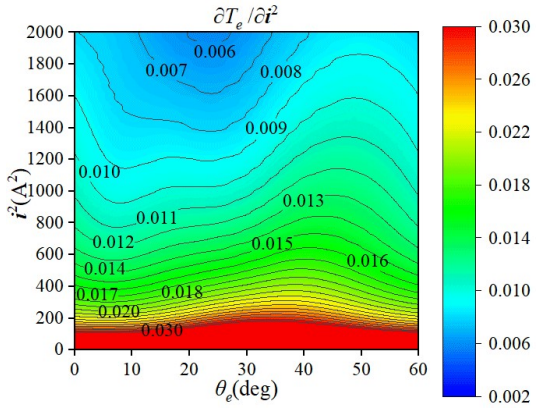

Fig. 5 $\partial T_e / \partial \boldsymbol{i}^2$ look-up table of forward torque by θ_e and $\boldsymbol{i}^2$ lookup.

$$F_1 = \int_0^{60} \left[T_e(\theta_e, f_1(\theta_e)) - T_e(\theta_e, f_2(\theta_e))\right]\mathrm{d}\theta_e / 60 \tag{16}$$

It is defined that $\theta_e \in a_1$ when $f_1(\theta_e) \geq f_2(\theta_e)$, that is a_1 is an interval that satisfies $f_1(\theta_e) \geq f_2(\theta_e)$. At this time, $\exists\, g_1(\theta_e) \in [f_2(\theta_e), f_1(\theta_e)]$ and $\exists\, \theta_{e1} \in a_1$ such that

$$\begin{aligned}
&\int_{a_1} \left[T_e(\theta_e, f_1(\theta_e)) - T_e(\theta_e, f_2(\theta_e))\right]\mathrm{d}\theta_e \\
&= \int_{a_1} \frac{\partial T_e}{\partial \boldsymbol{i}^2}(\theta_e, g_1(\theta_e))\left[f_1(\theta_e) - f_2(\theta_e)\right]\mathrm{d}\theta_e \\
&\geq \left[\frac{\partial T_e}{\partial \boldsymbol{i}^2}(\theta_e, g_1(\theta_e))\right]_{\min} \int_{a_1} \left[f_1(\theta_e) - f_2(\theta_e)\right]\mathrm{d}\theta_e \\
&= \frac{\partial T_e}{\partial \boldsymbol{i}^2}(\theta_e, g_1(\theta_{e1}))S_1
\end{aligned} \tag{17}$$

In a similar way, it is defined that $\theta_e \in a_2$ when $f_1(\theta_e) < f_2(\theta_e)$, that is a_2 is an interval that satisfies $f_1(\theta_e) < f_2(\theta_e)$. At this time, $\exists\, g_2(\theta_e) \in [f_1(\theta_e), f_2(\theta_e)]$ and $\exists\, \theta_{e2} \in a_2$ such that

$$\begin{aligned}
&\int_{a_2} \left[T_e(\theta_e, f_1(\theta_e)) - T_e(\theta_e, f_2(\theta_e))\right]\mathrm{d}\theta_e \\
&= -\int_{a_2} \frac{\partial T_e}{\partial \boldsymbol{i}^2}(\theta_e, g_2(\theta_e))\left[f_2(\theta_e) - f_1(\theta_e)\right]\mathrm{d}\theta_e \\
&> -\left[\frac{\partial T_e}{\partial \boldsymbol{i}^2}(\theta_e, g_2(\theta_e))\right]_{\max} \int_{a_2} \left[f_2(\theta_e) - f_1(\theta_e)\right]\mathrm{d}\theta_e \\
&= -\frac{\partial T_e}{\partial \boldsymbol{i}^2}(\theta_e, g_2(\theta_{e3}))S_2
\end{aligned} \tag{18}$$

It can be obtained from (15) that

$$\begin{aligned}
0 &= \int_{a_1} \left[f_1(\theta_e) - f_2(\theta_e)\right]\mathrm{d}\theta_e + \int_{a_2} \left[f_1(\theta_e) - f_2(\theta_e)\right]\mathrm{d}\theta_e \\
&= \int_{a_1} \left[f_1(\theta_e) - f_2(\theta_e)\right]\mathrm{d}\theta_e - \int_{a_2} \left[f_2(\theta_e) - f_1(\theta_e)\right]\mathrm{d}\theta_e = S_1 - S_2
\end{aligned} \tag{19}$$

From Fig. 5, it can be obtained that $\partial T_e / \partial \boldsymbol{i}^2$ is monotonically decreasing for $\boldsymbol{i}^2$. Thus for $g_1(\theta_{e1}) \leq f_1(\theta_e) < g_2(\theta_{e3})$ of (17) and (18), it is valid that

$$\frac{\partial T_e}{\partial i^2}(\theta_e, g_1(\theta_{e1})) \geq \frac{\partial T_e}{\partial i^2}(\theta_e, f_1(\theta_{e2})) > \frac{\partial T_e}{\partial i^2}(\theta_e, g_1(\theta_{e3})) \tag{20}$$

It can be obtained by (15)-(20) that

$$\begin{aligned} F_1 &> \left[\frac{\partial T_e}{\partial \boldsymbol{i}^2}(\theta_e, g_1(\theta_e))\right]_{\min} S_1 - \left[\frac{\partial T_e}{\partial \boldsymbol{i}^2}(\theta_e, g_2(\theta_e))\right]_{\max} S_2 \\ &= S_1\left\{\frac{\partial T_e}{\partial \boldsymbol{i}^2}(\theta_e, g_1(\theta_{e1})) - \frac{\partial T_e}{\partial \boldsymbol{i}^2}(\theta_e, g_1(\theta_{e3}))\right\} > 0 \end{aligned} \tag{21}$$

Therefore, when $T_e \geq 0$, the minimum torque cost curve is the contour line of $\partial T_e / \partial \boldsymbol{i}^2$.

Similarly, when the torque is reverse ($T_e < 0$), as shown in Fig. 6 and Fig. 7, the minimum torque cost curve is also the contour line of $\partial T_e / \partial \boldsymbol{i}^2$. The proof process is as follows.

The contour line $f_3(\theta_e)$ and the non-contour line $f_4(\theta_e)$ are taken in a torque period, which satisfy

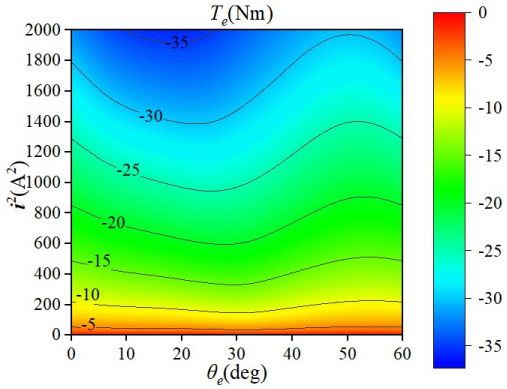

Fig. 6. Reverse torque look-up table by θ_e and $\boldsymbol{i}^2$ lookup.

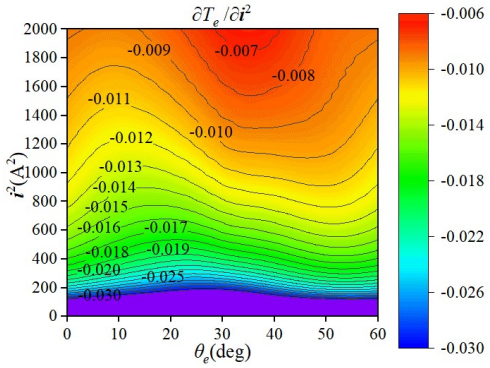

Fig. 7. $\partial T_e / \partial \boldsymbol{i}^2$ look-up table of reverse torque by θ_e and $\boldsymbol{i}^2$ lookup.

$$\int_0^{60} f_3(\theta_e)\mathrm{d}\theta_e / 60 = \int_0^{60} f_4(\theta_e)\mathrm{d}\theta_e / 60 \tag{22}$$

The difference F_2 of the T_e between the two curves can be expressed as

$$F_2 = \int_0^{60}\left[T_e(\theta_e, f_1(\theta_e)) - T_e(\theta_e, f_2(\theta_e))\right]\mathrm{d}\theta_e / 60 \tag{23}$$

It is defined that $\theta_e \in a_3$ when $f_3(\theta_e) \geq f_4(\theta_e)$, that is a_3 is an interval that satisfies $f_3(\theta_e) \geq f_4(\theta_e)$. At this time, $\exists\, g_3(\theta_e) \in [f_4(\theta_e), f_3(\theta_e)]$ and $\exists\, \theta_{e4} \in a_3$ such that

$$\begin{aligned} &\int_{a_3}\left[T_e(\theta_e, f_3(\theta_e)) - T_e(\theta_e, f_4(\theta_e))\right]\mathrm{d}\theta_e \\ &\leq \left[\frac{\partial T_e}{\partial \boldsymbol{i}^2}(\theta_e, g_1(\theta_e))\right]_{\max} \int_{a_3}\left[f_3(\theta_e) - f_4(\theta_e)\right]\mathrm{d}\theta_e \\ &= \frac{\partial T_e}{\partial \boldsymbol{i}^2}(\theta_e, g_3(\theta_{e4}))S_3 \end{aligned} \tag{24}$$

In a similar way, it is defined that $\theta_e \in a_4$ when $f_3(\theta_e) < f_4(\theta_e)$, that is a_4 is an interval that satisfies $f_3(\theta_e) < f_4(\theta_e)$. At this time, $\exists\, g_4(\theta_e) \in [f_3(\theta_e), f_4(\theta_e)]$ and $\exists\, \theta_{e6} \in a_4$ such that

$$\begin{aligned} &\int_{a_4}\left[T_e(\theta_e, f_3(\theta_e)) - T_e(\theta_e, f_4(\theta_e))\right]\mathrm{d}\theta_e \\ &< -\left[\frac{\partial T_e}{\partial \boldsymbol{i}^2}(\theta_e, g_4(\theta_e))\right]_{\min} \int_{a_4}\left[f_4(\theta_e) - f_3(\theta_e)\right]\mathrm{d}\theta_e \\ &= -\frac{\partial T_e}{\partial \boldsymbol{i}^2}(\theta_e, g_4(\theta_{e6}))S_4 \end{aligned} \tag{25}$$

It can be obtained from (22) that

$$S_3 = S_4 \tag{26}$$

From Fig. 7, it can be obtained that $\partial T_e / \partial \boldsymbol{i}^2$ is monotonically decreasing for $\boldsymbol{i}^2$. Thus for $g_3(\theta_{e4}) \leq f_3(\theta_e) < g_4(\theta_{e6})$ of (24) and (25), it is established that

$$\frac{\partial T_e}{\partial \boldsymbol{i}^2}(\theta_e, g_1(\theta_{e4})) \leq \frac{\partial T_e}{\partial \boldsymbol{i}^2}(\theta_e, f_1(\theta_{e5})) < \frac{\partial T_e}{\partial \boldsymbol{i}^2}(\theta_e, g_1(\theta_{e6})) \tag{27}$$

It can be obtained by (22)-(27) that

$$F < S_3\left\{\frac{\partial T_e}{\partial \boldsymbol{i}^2}(\theta_e, g_3(\theta_{e4})) - \frac{\partial T_e}{\partial \boldsymbol{i}^2}(\theta_e, g_3(\theta_{e6}))\right\} < 0 \tag{28}$$

Therefore, when $T_e < 0$, the minimum torque cost curve is also the contour line of $\partial T_e / \partial \boldsymbol{i}^2$. It can be seen from Fig.5 and Fig.7 that the contours correspond to variable $\boldsymbol{i}^2$, so the excitation currents for minimum torque cost is harmonic currents.

IV. Strategy Verification by the FEM

A. Comparison of Torque Response

In order to verify the effectiveness of the proposed strategy, the current shown in Fig. 8 is injected into the spoke-type PM motor. The subscripts '*f*' and '*r*' represent the forward and reverse torque, respectively, and the superscript '*c*' and '*p*' represents the conventional and proposed strategy, respectively. In Fig. 8, the two sinusoidal currents are obtained from the conventional strategy. And the harmonic currents are obtained from the proposed strategy in Fig. 5 and Fig. 7. The RMS values of the four currents in Fig. 8 are all the rate current of the spoke-type PM motor, where i_B and i_C lag i_A 120° and 240°, respectively.

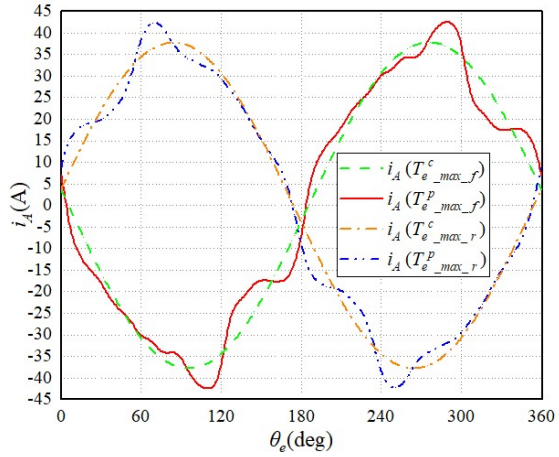

Fig. 8. Current excitation for maximum torque.

Excited by currents shown in Fig. 8, the FEM results of torque are shown in Fig. 9 and Fig. 10. It can be seen that the maximum torque of the forward and reverse torque increase by 1.40% and 1.22%, respectively, which means that the torque density is increased by the same percentage. It is worth mentioning that the forward and reverse torque of the spoke-type PM motor is different due to the influence of the flux linkage offset because of the auxiliary stator.

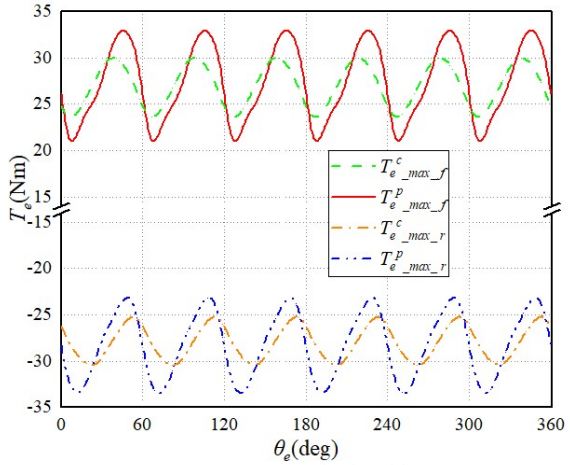

Fig. 9. Torque response comparison calculated by FEM.

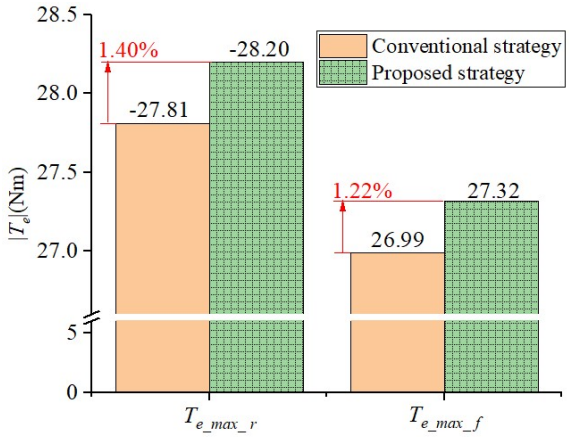

Fig. 10. Maximum torque comparison of the conventional and the proposed strategy.

B.Loss Analysis

The data in Table II represent the losses and energy flow in the motor, where P_{ed}, P_{hy}, P_{iron}, P_C, P_{out} represent copper loss, eddy current loss, hysteresis loss, iron loss, circuit electric power, output power, respectively. And these parameters satisfy the relation

$$P_{iron}=P_{ed}+P_{hy} \quad (29)$$

$$P_C=P_{out}+P_{iron} \quad (30)$$

$$P_{out}=T_e\times p\times\omega_e \quad (31)$$

When the motor outputs positive torque, energy flows from the circuit side to the output side, and the motor works in the electromotive state. At this time, P_C and P_{out} are positive. When the motor outputs negative torque, energy flows from the output side to the circuit side, and the motor works in the power generator state, which corresponds to the feed-back power braking operating state in the distributed drive systems. At this time, P_C and P_{out} are negative.

As shown in Table II, the iron loss of the proposed strategy increases compared to the conventional strategy, but this does not affect the effectiveness in terms of torque improvement.

TABLE II
POWER FLOW IN THE MOTOR

	P_{cu}/W	P_{ed}/W	P_{hy}/W	P_{iron}/W	P_C/W	P_{out}/W
$T_e^c{}_{max\_f}$	364	177	51	228	4751	4523
$T_e^p{}_{max\_f}$	364	215	55	270	4844	4574
$T_e^c{}_{max\_r}$	364	150	46	196	-4489	-4685
$T_e^p{}_{max\_r}$	364	180	51	231	-4493	-4724

V. EXPERIMENTAL VERIFICATION

In order to verify the effectiveness of the proposed strategy, the experiments are performed. The experimental platform is shown in Fig. 11. The accompanying PM synchronous motor (PMSM) was set to the speed of 30rpm. The spoke-type PM motor was excited with the given currents obtained from the proposed strategy using PIR controller, and the carrier frequency of PWM is 20kHz.

The measured current and torque response are shown in Fig. 12 and Fig. 13, respectively. The zero position of the waveforms is at the ground symbol of its same color. As shown in Fig. 14, it can be seen that the torque density of the forward and reverse maximum torque increase by 1.55% and 0.93%,

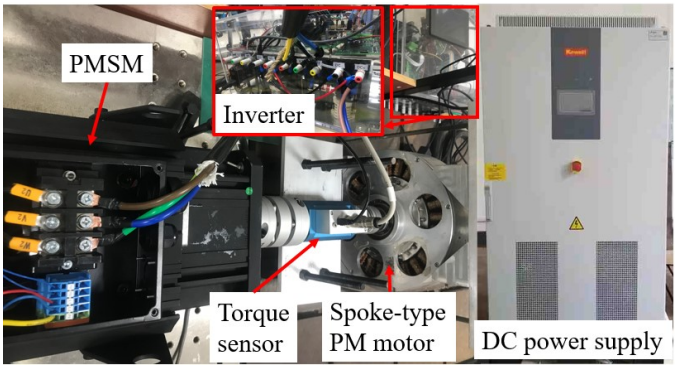

Fig. 11. Experiment platform.

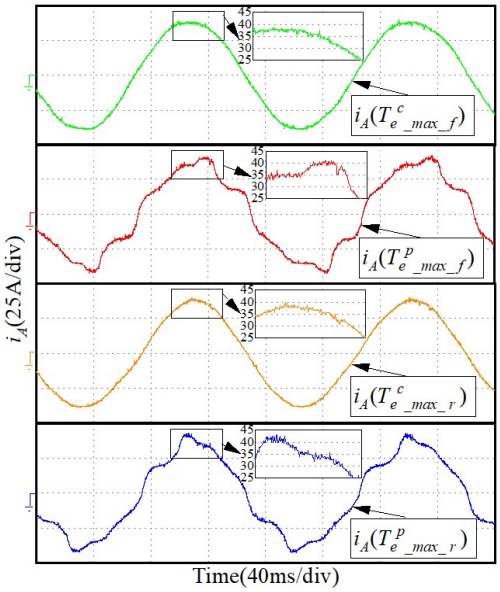

Fig. 12. Measured current waveforms of A phase.

respectively, which agrees well with the simulation results. The difference between the experiment and the simulation is presumably because there are inevitably mechanical tolerances in manufacturing and assembly difficulties in practice.

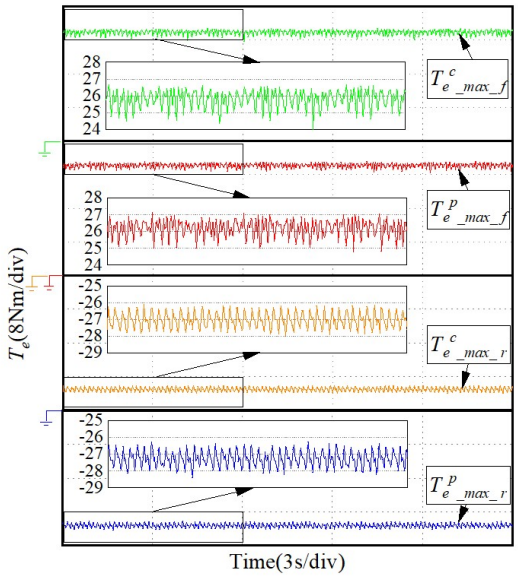

Fig. 13. Measured torque waveforms.

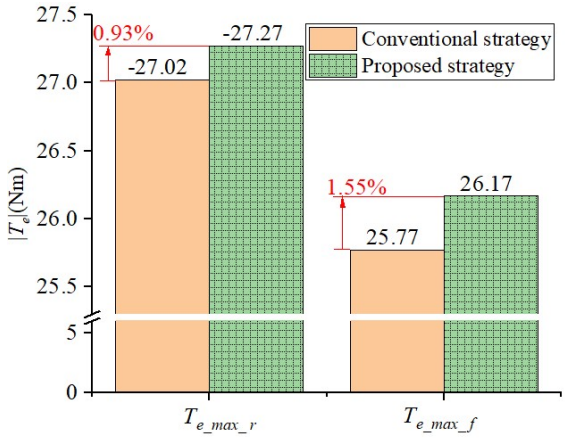

Fig. 14. Experimental comparison of forward and reverse maximum torque.

VI. Conclusion

This paper has proposed a strategy using harmonic currents to increase the torque density of the spoke-type PM motor with auxiliary stator, considering the magnetic field harmonics, cross-saturation effect and magnetic saturation. The conclusion was derived that the minimum torque cost curve is the $\partial T_e / \partial i^2$ contour line. The results by the FEM show that the torque density of the forward and reverse maximum torque increase by 1.22% and 1.40%, respectively. The experiment results show that the torque density of the forward and reverse maximum torque increase by 1.55% and 0.93%, respectively, which proves the effectiveness of the proposed strategy.

References

[1] C. S. Liu, Y. X. Xu, J. B. Zou, G. D. Yu, and L. Zhuo, "Permanent magnet shape optimization method for PMSM air gap flux density harmonics reduction," *CES Trans. Electr. Mach. Syst*., vol. 5, no. 4, pp. 284-290, Dec. 2021.

[2] Q. Chen, S. Eduku, and W. X. Zhao, "A new fault-tolerant switched flux machine with hybrid permanent magnets," *CES Trans. Electr. Mach. Syst.*, vol. 4, no. 2, pp. 79-86, Jun. 2020.

[3] W. X. Zhao, L. Xu, and G. H. Liu, "Overview of permanent-magnet fault-tolerant machines: topology and design," *CES Trans. Electr. Mach. Syst.,* vol. 2, no. 1, pp. 51-64, Mar. 2018.

[4] J. Q. Zheng, W. X. Zhao, C. H. T. Lee, J. H. Ji, and G. H. Xu, "Improvement torque performances of interior permanent-magnet machines," *CES Trans. Electr. Mach. Syst.*, vol. 3, no. 1, pp. 12-18, Mar. 2019.

[5] Z. Y. Liang, Y. T. Gao, D. W. Li, and Q. R. Qu, "Design of a novel dual flux modulation machine with consequent-pole spoke-array permanent magnets in both stator and rotor," *CES Trans. Electr. Mach. Syst.*, vol. 2, no. 1, pp. 73-81, Mar. 2018.

[6] W. L. Zhao, T. A. Lipo, and B. Kwon, "Torque pulsation minimization in spoke-type interior permanent magnet motors with skewing and sinusoidal permanent magnet configurations," *IEEE Trans. Magn*., vol. 51, no. 11, Jan. 2015.

[7] D. G. Dorrell, M. Hsieh, and A. M. Knight, "Alternative rotor designs for high performance brushless permanent magnet machines for hybrid electric vehicles," *IEEE Trans. Magn*., vol. 48, no. 2, pp. 835-838, Jan. 2012.

[8] M. M. Rahman, K. Kim, and J. Hur, "Design and optimization of neodymium-free spoke-type motor with segmented wing-shaped PM," *IEEE Trans. Magn*., vol. 50, no. 2, pp. 865-868, Jan. 2014.

[9] M. Ehsani, K. M. Rahman, and H. Toliyat, "Propulsion system design of electric and hybrid vehicles," *IEEE Trans. Ind. Electron*., vol. 44, no. 1, pp. 19-27, Feb. 1997.

[10] C. Liu, K. T. Chau, and J. Z. Jiang, "A permanent-magnet hybrid in-wheel motor drive for electric vehicles," *IEEE Veh. Power Propul. Conf*., pp. 1-6, 2008.

[11] Y. Feng, F. Li, S. Huang, and N. Yang, "Variable-flux outer-rotor permanent magnet synchronous motor for in-wheel direct-drive applications," *Chin. J. Electr. Eng*., vol. 4, no. 1, pp. 28-35, Mar. 2018.

[12] W. L. Zhao, J. Kwon, X. H. Wang, T. A. Lipo, and B. Kwon, "Optimal design of a spoke-type permanent magnet motor with phase-group concentrated-coil windings to minimize torque pulsations," *IEEE Trans. Magn*., vol. 53, no. 6, pp. 1-4, Jan. 2017.

[13] X. H. Kong, Y. T. Hua, Z. R. Zhang, C. Wang, and Y. Liu, "Analytical modeling of high-torque-density spoke-type permanent magnet in-wheel motor accounting for rotor slot and eccentric magnetic pole," *IEEE Trans. Transp. Electrif*., vol. 7, no. 4, pp. 2683-2693, Jan. 2021.

[14] M. N. Uddin, T. s. Radwan, and M. A. Rahman, "Performance of Interior Permanent Magnet Motor Drive Over Wide Speed Range," *IEEE Trans. Energ. Convers*., vol. 17, no. 1, pp. 79-84, Mar. 2002.

[15] C. T. Pan, and S. M. Sue, "A Linear Maximum Torque Per Ampere Control for IPMSM Drives Over Full-speed Range," *IEEE Trans. Energ. Convers.*, vol. 20, no. 2, pp. 359-366, Jun. 2005.

[16] H. S. Kim, Y. Lee, S. K. Sul, J. Yu, and J. Oh, "Online MTPA Control of IPMSM Based on Robust Numerical Optimization Technique," *IEEE Trans. Ind. Appli*., vol. 55, no. 4, pp. 3736-3746, Aug. 2019.

[17] A. Shinohara, Y. Inoue, S. Morimoto and M. Sanada, "Maximum Torque Per Ampere Control in Stator Flux Linkage Synchronous Frame for DTC-based PMSM Drives Without Using q-axis Inductance," *IEEE Trans. Ind. Appli.*, vol. 53, no. 4, pp. 3663-3671, Aug. 2017.

[18] Z. Xia, S. Nalakath, R. Tarvirdilu-Asl, Y. Sun, J. Wiseman and A. Emadi, "Online Optimal Tracking Method for Interior Permanent Magnet Machines with Improved MTPA and MTPV in Whole Speed and Torque Ranges," *IEEE Trans. Power Electron*., vol. 35, no. 9, pp. 9753-9769, Sept. 2020.

[19] T. D. Do, S. Kwak, H. H. Choi and J. Jung, "Suboptimal Control Scheme Design for Interior Permanent-magnet Synchronous Motors: an SDRE-based Approach," *IEEE Trans. Power Electron*., vol. 29, no. 6, pp. 3020-3031, Jun. 2014.

[20] C. B. Butt and M. A. Rahman, "Untrained Artificial Neuron-based Speed Control of Interior Permanent-magnet Motor Drives Over Extended Operating Speed Range," *IEEE Trans. Ind. Appli*., vol. 49, no. 3, pp. 1146-1153, Jun. 2013.

[21] K. Lee, S. Park and S. Jeong, "A Seamless Transition Control of Sensorless PMSM Compressor Drives for Improving Efficiency Based on

a Dual-Mode Operation," *IEEE Trans. Power Electron.*, vol. 30, no. 3, pp. 1446-1456, Mar. 2015.

[22] B. Y. Zheng, J. B. Zou, Y. X. Xu, L. Y. Lang, and G. D. Yu, "Torque ripple suppression based on optimal harmonic current injection in dual three-phase PMSMs under magnetic saturation," *IEEE Trans. Ind. Electron.*, vol. 69, no. 6, pp. 5398-5408, Jun. 2022.

[23] Z. X. Yu, D. W. Li, W. B. Kong, R. H. Qu, S. F. Jia, D. Jiang, and Y. Zhou, "New optimal current control strategy for six-phase DC-biased vernier reluctance machines considering distorted EMF," *IEEE Trans. Power Electron.*, vol. 33, no. 12, pp. 10633-10645, Dec. 2018.

[24] Z. X. Yu, W. B. Kong, R. H. Qu, Z. M. Li, and D. W. Li, "Dual-inverter PWM scheme for DC-biased vernier reluctance machines with reduced switching frequency capable of zero sequence current regulation," *IEEE Trans. Ind. Electron.*, vol. 69, no. 2, pp. 1276-1287, Feb. 2022.

[25] X. Q. Wang, Z. Wang, M. R. Gu, B. Wang, W. Wang, and M. Cheng, "Current optimization-based fault-tolerant control of standard three-phase PMSM drives," *IEEE Trans. Energy Convers.*, vol. 36, no. 2, pp. 1023-1035, Jun. 2021.

[26] G. D. Yu, Y. X. Xu, J. B. Zou, L. J. Xiao, and B. Y. Zheng, "Modeling and analysis of limited-angle torque motor considering nonlinear effects," *IEEE Trans. Transp. Electrification*, vol. 6, no. 4, pp. 1457-1465, Dec. 2020.

[27] J. Lee, Y. -C. Kwon and S. -K. Sul, "Identification of IPMSM Flux-Linkage Map for High-Accuracy Simulation of IPMSM Drives," *IEEE Trans. Power Electron.*, vol. 36, no. 12, pp. 14257-14266, Dec. 2021.

[28] X. Chen, J. Wang, B. Sen, P. Lazari and T. Sun, "A High-Fidelity and Computationally Efficient Model for Interior Permanent-Magnet Machines Considering the Magnetic Saturation, Spatial Harmonics, and Iron Loss Effect," *IEEE Trans. Ind. Electron.*, vol. 62, no. 7, pp. 4044-4055, July 2015.

[29] D. Hu, Y. M. Alsmadi and L. Xu, "High-Fidelity Nonlinear IPM Modeling Based on Measured Stator Winding Flux Linkage," *IEEE Trans. Ind. Appli.*, vol. 51, no. 4, pp. 3012-3019, July-Aug. 2015.

Hao Wu was born in China on December 1998. He received the B.S. degree in electrical engineering and automation from China University of Mining and Technology, Xuzhou, China, in 2020. He is currently working toward the M.E degree in the School of Electrical Engineering, Shandong University, Jinan, China.

His current research interests include design, analysis and control of electrical machines.

Wenliang Zhao (S'14–M'16) was born in China on May 1987. He received the B.S. degree in control science and engineering from Harbin Institute of Technology, China, in 2011, and the Ph.D. degree in electronic systems engineering from Hanyang University, South Korea, in 2015.

From 2015 to 2016, he was a Postdoctoral Fellow with Hanyang University, South Korea. In 2016, he joined the School of Electrical Engineering, Shandong University, as a Research Professor. Since 2020, he has been a Full Professor of Shandong University. He has authored or coauthored more than 100 papers on the topics of his research interests, which include design, analysis and control of electrical machines and power transformers.

Zheng Li was born in China on March 1987. He received the M.E degree in software engineering from Shandong University, Jinan, China, in 2014.

He is currently working in Jinan Heating Group CO. LTD., mainly engaged in the field of industrial automation and enterprise information construction.

Xiuhe Wang was born in China on July 1967. He received the B.E. and M.E. degrees from Shandong University, Jinan, China, in 1989 and 1993, respectively, and the PhD degree from Shenyang University of Technology, Shenyang, China, in 1996.

From 2001 to 2002, he was a Postdoctoral Fellow with Seoul National University, Seoul, South Korea. He is currently a Professor of electrical engineering and the Vice Head of the School of Electrical Engineering, Shandong University. His research interests include permanent magnet machines, energy-efficient machines, theoretical analysis and calculation of electromagnetic devices, and their application on electrical machines. He has authored/co-authored more than 100 papers on these topics.